RSC Advances

RSC Publishing

PAPER

View Article Online
View Journal | View Issue

Cite this: *RSC Advances*, 2013, **3**, 18573

Template-engaged synthesis of uniform mesoporous hollow $NiCo_2O_4$ sub-microspheres towards high-performance electrochemical capacitors†

Changzhou Yuan,*[a] Jiaoyang Li,[a] Linrui Hou,[a] Jingdong Lin,*[b] Gang Pang,[ac] Longhai Zhang,[a] Lin Lian[a] and Xiaogang Zhang[c]

Received 7th June 2013,
Accepted 5th August 2013

DOI: 10.1039/c3ra42828a

www.rsc.org/advances

An efficient template-engaged synthetic strategy, where silica spheres were applied as hard templates, was developed to synthesize hierarchical mesoporous hollow $NiCo_2O_4$ sub-microspheres assembled entirely from ultrathin nanosheets with a thickness of a few nanometers. The as-prepared mesoporous hollow $NiCo_2O_4$ sub-microspheres are very uniform in size, mesoporous in textual property, and structurally robust benefiting from the *in situ* template removal. The morphologies of the hollow sub-microspherical architecture can be tuned easily by varying the concentrations of Ni^{2+}, Co^{2+}, and the precipitant. When evaluated as an appealing electroactive material for electrochemical capacitors (ECs), the as-fabricated hierarchical hollow $NiCo_2O_4$ sub-microspheres delivered a specific capacitance (SC) of 678 F g^{-1} at a current density of 1 A g^{-1}, and even kept it as high as 540 F g^{-1} at 10 A g^{-1}. Additionally, a desirable cycling stability of 13% SC degradation over 3500 continuous cycles at a current density of 10 A g^{-1} is observed, suggesting their promising application in advanced ECs.

1. Introduction

Recently, a low-cost binary metal oxide, spinel $NiCo_2O_4$, has sparked worldwide concern as an appealing pseudocapacitive electrode for advanced electrochemical capacitor (ECs) applications.[1–16] The unique cobaltite possesses a general formula of $Co^{2+}{}_{1-x}Co^{3+}{}_x[Co^{3+}Ni^{2+}{}_xNi^{3+}{}_{1-x}]O_4$ ($0 < x < 1$), where the Ni species occupies the octahedral sites and the Co is distributed over both octahedral and tetrahedral sites, as seen from Fig. 1a. Due to the presence of mixed valences of the same cation in such spinel cobaltite, the $NiCo_2O_4$ possesses at least two orders of magnitude higher electrical conductivity than monometallic nickel and cobalt oxides because of electron transfer taking placing with relatively low activation energy between cations.[1,17,18] It is documented to have 62 S cm^{-1} for a single crystal $NiCo_2O_4$ nanoplate at room temperature (RT),[17] and 0.6 S cm^{-1} for a polycrystalline $NiCo_2O_4$ film at 300 °C.[18] Besides this, rich redox reactions, originating from both nickel and cobalt ions, render its EC application intriguing as a scalable alternative pseudocapacitive electrode.[1–16] Hu *et al.*[1] first reported the $NiCo_2O_4$ aerogels synthesized *via* the simple epoxide-driven sol–gel process and the as-fabricated aerogels delivered an extremely high specific capacitance (SC) of 1400 F g^{-1} after 650-cycle activation. Following this impressive and pioneering contribution, various low-dimensional $NiCo_2O_4$ nanostructures, including 1D porous nanowires (NWs) and nanoneedles,[2–7] 2D nanosheets (NSs),[5,8,9] platelet-like nanoparticles (NPs),[10] coral-like porous crystals,[11] ordered mesoporous particles,[12] porous network-like frameworks,[13] and even several urchin-like micro-/nanostructures[14–16] have been intensively fabricated as attractive pseudocapacitive materials for high-performance ECs.

Nevertheless, there are far fewer reports on the fabrication of elegant hollow $NiCo_2O_4$ micro-/nanostructures with large

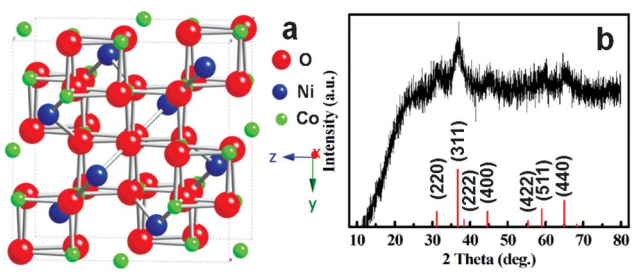

Fig. 1 (a) Crystal structure of $NiCo_2O_4$ unit cell with the spinel structure. (b) wide-angle XRD pattern of the as-synthesized mesoporous hollow $NiCo_2O_4$ sub-microspheres.

[a]*School of Materials Science & Engineering, Anhui University of Technology, Ma'anshan, 243002, P. R. China. E-mail: ayuancz@163.com*
[b]*Department of Chemistry, College of Chemistry and Chemical Engineering, Xiamen University, Xiamen, 361005, P. R. China. E-mail: jdlin@xmu.edu.cn*
[c]*College of Material Science and Engineering Nanjing University of Aeronautics and Astronautics, Nanjing, 210016, P. R. China*

† Electronic supplementary information (ESI) available: FESEM and TEM images of the controlled experiments, electrochemical performance of the $NiCo_2O_4$-1 and $NiCo_2O_4$-2 samples. See DOI: 10.1039/c3ra42828a

specific surface area (SSA), convenient short ion and electron diffusion paths, and desirable hierarchical porosity (*i.e.*, meso- and macro-porosity) for next-generation EC applications so far. It is well established that in regard to the higher-level micro-/nanostructures, typically of micro-/sub-micrometer dimensions but internally consisting of nano-building blocks and/or nano-domains, they can offer the exceptional advantages of both nanometer-sized building blocks/nano-domains (NPs, NWs, NSs, *etc.*) and micro-/sub-micrometer-sized assemblies themselves.[19–22] And as for the hierarchical porosity, the mesopores possess the ability to hold the electrolyte and prevent it from over-flooding under the capillary force for ensuring high energy-storage ability, and the macropores of the interior cavities, serving as the ''ion-buffering reservoirs'', minimize the diffusion distance to the interior surfaces, which may accelerate the kinetic process of the ion diffusion in the electrode, hence exhibiting a striking electrochemical capacitance.[19–21,23] Furthermore, the permeable thin shells afford greatly reduced paths both for ion and electron diffusion, leading to even better rate capability. Therefore, it is still of great significance but challenging to develop a low-cost and scalable approach for the efficient synthesis of $NiCo_2O_4$ hollow micro-/nanostructures with unique and hierarchical structures.

Herein, we report the template-assisted synthesis of ultrathin NS-constructed mesoporous hollow $NiCo_2O_4$ micro-/nanostructures by using silica spheres as a template. In addition, the effect of the specific experimental parameters on the robust mesoporous hollow structure of the hierarchical sub-microspheres also has been systematically investigated. When evaluated as a potential pseudocapacitive electrode for advanced ECs, the as-synthesized mesoporous hollow $NiCo_2O_4$ sub-microspheres delivered large SCs and remarkable long-term cycling stability at large current densities.

2. Experimental

2.1 Materials synthesis

Silica spherical particles were prepared by the modified Stöber method.[24,25] The obtained silica spheres were re-dispersed into 30 mL of a mixed solution of ethanol (15 mL), de-ionized (DI) water (15 mL) and hydroxypropyl cellulose (HPC, 0.05 g). After ultrasonication for 30 min, 0.5 mM of $Ni(NO_3)_2{\cdot}6H_2O$, 1 mM of $Co(NO_3)_2{\cdot}6H_2O$ and 4 mM of urea were dissolved into the above mixture. Then, the mixture was refluxed at 80 °C for 3 h under stirring. After being cooled down to RT naturally, the product was collected, washed, dried and calcined at 300 °C for 1 h and the resultant sample was further added into 100 mL of 3 M NaOH solution. After being stirred at RT for 24 h, the product was collected through centrifugation, washed with DI water and ethanol several times, dried and further calcined at 300 °C for 0.5 h with a slow heating rate of 1 °C min^{-1}. For comparison, different concentrations of Ni^{2+}, Co^{2+} and urea were applied in the synthesis of other $NiCo_2O_4$ samples. The sample was designated as $NiCo_2O_4$-1 when 0.25 mM of $Ni(NO_3)_2{\cdot}6H_2O$, 0.5 mM of $Co(NO_3)_2{\cdot}6H_2O$ and 2 mM of urea were used. When 0.75 mM of $Ni(NO_3)_2{\cdot}6H_2O$, 1.5 mM of $Co(NO_3)_2{\cdot}6H_2O$ and 6 mM of urea were applied, the obtained sample was then designated as $NiCo_2O_4$-2 accordingly.

2.2 Materials characterization

Crystallographic phases of the product were investigated by powder X-ray diffraction (Bruker, D8-Advance XRD, Cu-Kα, λ = 1.5406 Å) at a scanning speed of 3° min^{-1} over a 2θ range of 10–80°. The morphologies and structures of the resultant samples were observed by field-emission scanning electron microscopy(FESEM, JEOL-6300F, 15 kV), transmission electron microscopy (TEM), high-resolution TEM (HRTEM), energy dispersive X-ray analysis (EDXA), and selected area electron diffraction (SAED) (JEOL JEM 2100 system operating at 200 kV). Measurement of SSA and analysis of porosity for the $NiCo_2O_4$ products were performed through measuring N_2 adsorption–desorption isotherms at 77 K with an ASAP-2010 surface area analyzer.

2.3 Electrochemical measurements

The working electrodes were prepared with the electroactive material $NiCo_2O_4$, acetylene black (AB) and polytetrafluoroethylene (PTFE) in a weight ratio of 8 : 1.5 : 0.5. A small amount of 3 M KOH was then added to make a more homogeneous mixture, which was pressed on nickel foam with a surface area of 1 cm^2 ($\sim 10^7$ Pa) for the following electrochemical tests by cyclic voltammetry (CV) and chronopotentiometry (CP) measurements performed with an IVIUM electrochemical workstation (the Netherlands). The typical loading of the electroactive $NiCo_2O_4$ was 8 mg cm^{-2}. All experiments were carried out in a three-electrode system with a working electrode, a platinum plate counter electrode (1 cm^2) and a saturated calomel electrode (SCE) reference electrode at RT. The electrolyte used here was 3 M KOH aqueous solution. The cycling performance was carried out with a CT2001D tester (Wuhan, China). The SCs of the $NiCo_2O_4$ electrodes can be calculated by using eqn (1):

$$C_s = \frac{It}{\Delta V} \quad (1)$$

where C_s is the specific capacitance (F g^{-1}) of the $NiCo_2O_4$ electrodes, I donates the discharge current (A g^{-1}), t is the discharging time (s), and ΔV is the discharge potential interval (V). In addition, another important parameter, columbic efficiency (η) of the electrodes, was evaluated from eqn (2):

$$\eta = \frac{t_D}{t_C} \times 100\% \quad (2)$$

where t_D and t_C are the time for galvanostatic discharging and charging, respectively.

3. Results and discussion

3.1 Physicochemical characterization

The crystallographic phase of the as-fabricated $NiCo_2O_4$ product was studied by the XRD technique, and the typical wide-angle diffraction pattern is shown in Fig. 1b. Seven well-

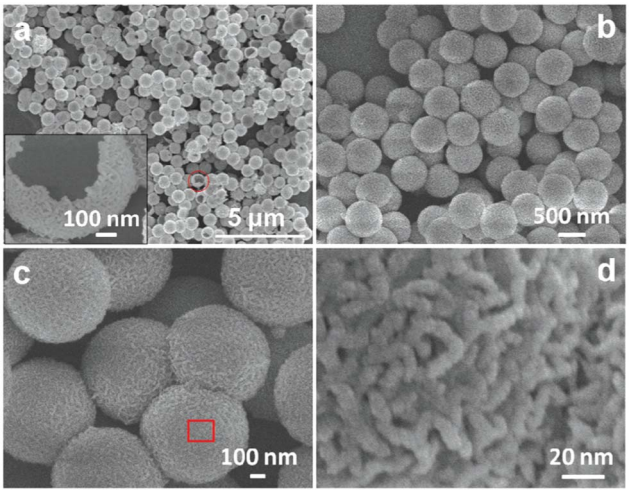

Fig. 2 (a–d) FESEM images with different magnifications for the hollow $NiCo_2O_4$ sub-microspheres. The inset in panel a in an enlargement of the part indicated by the circle in panel a. The image in (d) is taken from the region marked with the rectangle in panel c.

defined diffraction peaks, including not only the peak position, but also their relative intensities, can be observed, and easily indexed as a cubic spinel $NiCo_2O_4$ crystalline structure (JCPDF file no. 20-0781; space group: F*3 (202)), as seen from the standard spectra indicated by the red lines in Fig. 1b. The relatively broad diffraction peaks with low intensity could be ascribed to the typical nanocrystalline characteristic of the as-obtained $NiCo_2O_4$ sample.[26]

Fig. 2 presents the representative FESEM images of the resultant $NiCo_2O_4$. The low-magnification FESEM images (Fig. 2a and b) reveal that the product is composed of uniform mono-dispersed sub-microspheres with a diameter of ~650 nm, which inherits well the original spherical shape of the silica templates with a size of 600–700 nm (Fig. S1, ESI†). Of particular note is that no free simple $NiCo_2O_4$ NPs can be found. It demonstrates the uniform coating of all the $NiCo_2O_4$ on the entire surface of the silica spheres, and with the subsequent gradual removal of the silica template in the alkaline NaOH environment, the structural integrity remains well without losing the spherical morphology. When focusing on a few of the spheres with cracked shells, it could be observed that the round spherical particles have hollow cavities. Particularly, a representative broken $NiCo_2O_4$ microsphere is displayed (the inset in Fig. 2a), where the hollow interior can be identified unambiguously from the broken part. More interestingly, careful examination reveals that the surface of the $NiCo_2O_4$ sub-microspheres is quite rough (Fig. 2c and d) and some evident "wrinkles" with a thickness of ~4 nm can be clearly seen under higher magnifications (Fig. 2d), which would be favorable for obtaining much more electroactive sites for efficient electrochemical energy storage.

The hollow interior and geometrical structure of as-synthesized $NiCo_2O_4$ sub-microspheres are further elucidated by (HR)TEM examination. In good agreement with the above SEM finding, a high uniformity of the hollow spheres can be observed from the images, as displayed in Fig. 3a and b, and

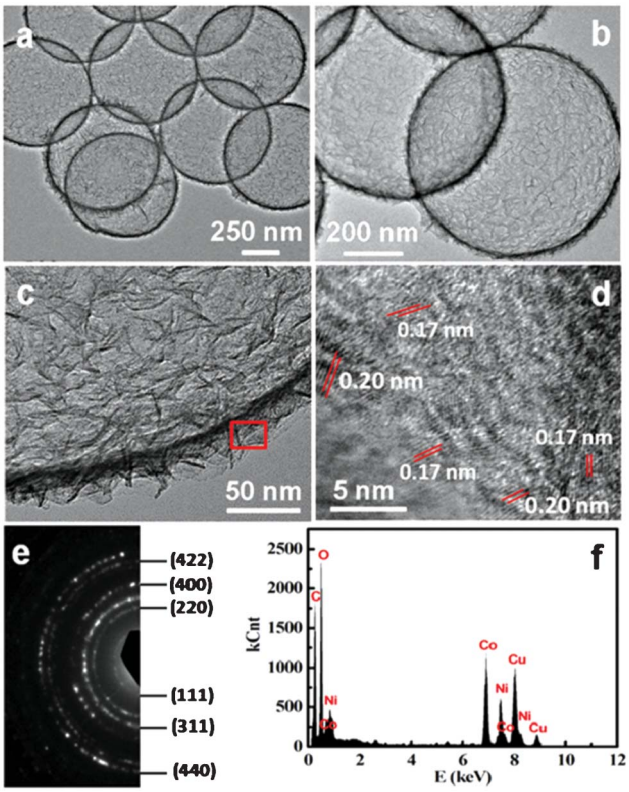

Fig. 3 (a–c) TEM and (d) HRTEM images, (e) SAED pattern and (f) EDAX of the hollow $NiCo_2O_4$ sub-microspheres. The image in (d) is taken from the region marked with the rectangle in panel c.

the inner cavity is clearly revealed by the sharp contrast between the shell and hollow interior in the images. The thickness of the shell is ~25 nm. No apparent collapse of the shell is observed owing to the good structural stability and integrity of the hollow spheres. As demonstrated in Fig. 3c, the hierarchical hollow sub-microspheres are constructed by lots of delicate NSs as the subunits, and also the presence of ultrathin NSs around the shell, of which the thickness is as low as a few nanometers, can be found. It is due to the existence of these ultrathin NSs that the $NiCo_2O_4$ sub-microspheres with wrinkle-like rough surfaces are evident (Fig. 2d). Further HRTEM observation (Fig. 3d) evidences the obviously resolved lattice fringes, which were calculated to be ~0.17 and 0.20 nm, corresponding to the (220) and (311) planes of spinel structured $NiCo_2O_4$, respectively. The SAED pattern (Fig. 3e), detected from a sampling area indicated by the red rectangle in Fig. 3c, shows well-defined diffraction rings, revealing its typical polycrystalline characteristics, and the diffraction rings can be readily indexed to the (111), (220), (311), (400), (422), (440) planes of the $NiCo_2O_4$ phase, respectively, which is consistent with the above XRD result (Fig. 1b). The chemical composition of the $NiCo_2O_4$ hollow sub-microspheres is further confirmed by the EDAX data (Fig. 3f), which shows a Ni/Co ratio of ~1/2. Moreover, no discernible Si species can be found, indicating the complete removal of the silica template after stirring in 3 M NaOH solution for 24 h at RT, and the consequent formation of the pure $NiCo_2O_4$ phase.

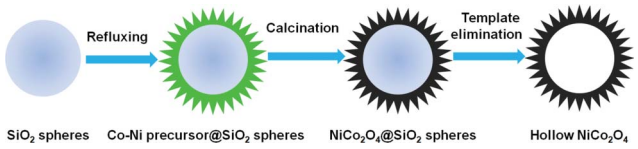

Fig. 4 Schematic illustration of the formation of the mesoporous hollow $NiCo_2O_4$ sub-microspheres.

As shown in Fig. 4, during the refluxing procedure, the Co–Ni precursor was uniformly coated upon the surface of the Si template, and the $NiCo_2O_4$ was formed after calcination. With the subsequent gradual removal of the silica template in alkaline NaOH aqueous solution, the mesoporous hollow $NiCo_2O_4$ sub-microspheres were finally obtained. Interestingly, if the concentrations of Ni^{2+}, Co^{2+} and urea applied in the refluxing procedure were changed while the other conditions kept the same, different $NiCo_2O_4$ samples with distinct morphologies would be obtained. In regard to the $NiCo_2O_4$-1 sample (Fig. S2a and b, ESI†), which was fabricated by using 0.25 mM of $Ni(NO_3)_2{\cdot}6H_2O$, 0.5 mM of $Co(NO_3)_2{\cdot}6H_2O$ and 2 mM of urea, evidently, the hollow architecture cannot be observed, and nearly all of them collapse. Owing to the low concentrations of these reactants, a small quantity of $NiCo_2O_4$ was first grown upon the surfaces of the silica template under otherwise identical conditions. Upon the subsequent removal of the silica template, the obtained $NiCo_2O_4$ shell is too thin to guarantee the stability and integrity of the hollow spherical architecture, and consequently, total collapse occurs, while for the $NiCo_2O_4$-2, which was synthesized by using 0.75 mM of $Ni(NO_3)_2{\cdot}6H_2O$, 1.5 mM of $Co(NO_3)_2{\cdot}6H_2O$ and 6 mM of urea, adherent hollow sub-microspheres with even thicker shells of ~110–116 nm were observed (Fig. S2c, ESI†). In common, the higher concentrations of the reactants lead to fast nuclear and rapid growth, thus the hollow sub-microspheres with mutual adhesion are formed. Also of particular note, if just etched for 20 h in 3 M NaOH at RT, some small silica templates still can be found (Fig. S3, ESI†), therefore, the much longer etching time of 24 h is needed to completely remove the silica template. All in all, the concentration of the reactants and etching time plays a significant role in fabricating the mono-dispersed hierarchical $NiCo_2O_4$ sub-microspheres with perfect integrity and high purity.

To more clearly describe the porous properties and textural properties of the as-fabricated mono-dispersed hierarchical $NiCo_2O_4$ hollow sub-microspheres, N_2 adsorption–desorption measurements were further applied. The adsorption isotherms of the unique $NiCo_2O_4$ sub-microspheres are shown in Fig. 5a. The isotherm can be classified as type IV according to the International Union of Pure and Applied Chemistry classification. Notably, a distinct hysteresis loop can be observed in the larger range of ~0.5–1.0 P/P_0, suggesting that the as-prepared $NiCo_2O_4$ sub-microspheres have a typical mesoporous structure, which can be further supported by the Barrett–Joyner–Halenda (BJH) pore size distribution (PSD) (Fig. 5b). Evidently, the pore distribution is relatively narrow, and mainly centered in the range of 3–5 nm. Moreover, the BET SSA, average pore size and mesopore volume of the unique mesoporous hollow

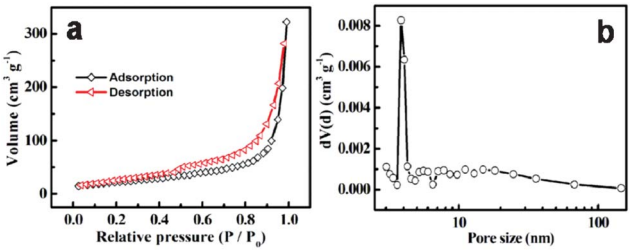

Fig. 5 (a) N_2 adsorption–desorption isotherms and (b) PSD of the mesoporous hollow $NiCo_2O_4$ sub-microspheres.

$NiCo_2O_4$ sub-microspheres are quantitatively summarized as 116 $m^2\ g^{-1}$, 3.8 nm and 0.51 $cm^3\ g^{-1}$, respectively. Apparently, such a unique hierarchical hollow structure with intriguing mesoporosity and large SSA holds significant promise in offering sufficient surface/interface electroactive sites to facilitate more electrochemical reactions in the redox process with respect to their bulk or solid counterparts, and consequently, provides high SC even at large current densities.

3.2 Electrochemical properties

For the sake of confirming the potential application of the as-fabricated hierarchical mesoporous hollow $NiCo_2O_4$ sub-microspheres in high-performance ECs, next the product was configured as pseudocapacitive electrodes in a three-electrode cell to evaluate their electrochemical properties. Potential sweep CV measurement was employed to characterize the capacitive performance of the $NiCo_2O_4$ electrodes, and typical CV curves are depicted in Fig. 6. The voltage was swept from −0.1 to 0.4 V (*vs.* SCE) at various scanning rates ranging from 5 mV to 20 mV s^{-1}. Evidently, the electrochemical response currents of the CV curves on the positive sweeps are nearly mirror-image symmetric to their corresponding counterparts on the negative sweeps with respect to the zero-current line. In addition, as the scan rate increases from 5 to 20 mV s^{-1}, the current subsequently increases while the CV shape changes little, and rapid current response on voltage reversal occurs at each end potential at all the scanning rates, which indicates its intriguing electrochemical capacitive nature. The CV curve shapes with a couple of redox peaks reveal that the capacitive

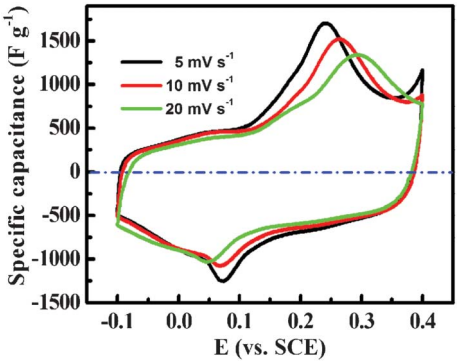

Fig. 6 Typical CV curves of the mesoporous hollow $NiCo_2O_4$ sub-microspheres at various scan rates.

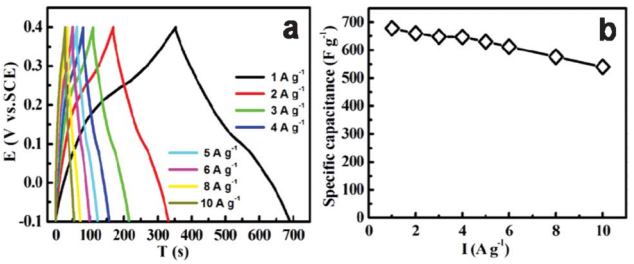

Fig. 7 (a) CP plots at various current density, and (b) calculated SC as a function of current density of the mesoporous hollow $NiCo_2O_4$ sub-microspheres.

characteristics of the mesoporous hollow $NiCo_2O_4$ sub-microspheres are distinct from those of electric double-layer capacitance (EDLC), in which the shape is normally close to an ideal rectangular shape. The well defined redox peaks within the potential scanning range mainly resulted from redox reactions related to M–O/M–O–OH (M = Co and Ni ions) in the alkaline electrolyte, as shown in eqn (3) and (4):[27–31]

$$NiCo_2O_4 + OH^- + H_2O \leftrightarrow NiOOH + 2CoOOH = 2e^- \quad (3)$$

$$CoOOH + OH^- \leftrightarrow CoO_2 + H_2O + e^- \quad (4)$$

To further quantify the SCs, the galvanostatic charge–discharge plots of the mesoporous hollow $NiCo_2O_4$ sub-microspheres within a potential window of −0.1 to 0.4 V (*vs.* SCE) at various current densities ranging from 1 to 10 A g^{-1} were measured for the same electrode used in the CV measurement above, and are depicted in Fig. 7a. The observation of nearly symmetric *E*–*t* curves at all current densities implies the high charge–discharge coulombic efficiency and low polarization of the unique mesoporous hollow $NiCo_2O_4$ sub-microsphere electrode. The SCs of the unique mesoporous hollow electrode can be calculated based on the charge–discharge curves in Fig. 6a and the typical results are collected in Fig. 7b. Impressively, the mesoporous hollow electrode exhibits excellent pseudocapacitance of 678, 660, 648, 647, 630, 612, 576 and 540 F g^{-1} at current densities of 1, 2, 3, 4, 5, 6, 8 and 10 A g^{-1}, respectively. This suggests that ~79.6% of the capacitance is still retained when the charge–discharge rate increases to 10 from 1 A g^{-1}, which highlights the prominent application of the mesoporous hollow sub-microspheres in ECs serving as an excellent electroactive material, due to their strong ability to provide high power and maintain striking SCs at a high charge/discharge rate. Furthermore, it is worthy of note that the electrochemical performance of the mesoporous hollow $NiCo_2O_4$ sub-microspheres is even better than those of the $NiCo_2O_4$-1 and $NiCo_2O_4$-2 samples in terms of SCs or SC retention at high rates (Fig. S4, ESI†). Specifically, as for the $NiCo_2O_4$-1 electrode, a SC of 662 F g^{-1} can be delivered at a current density of 1 A g^{-1}, which is somewhat comparable with that of the mesoporous hollow $NiCo_2O_4$ sub-microsphere electrode, however, when the current is up to 10 A g^{-1}, a SC of 473 F g^{-1}, *i.e.*, ~71% SC retention, is just obtained. As regards the $NiCo_2O_4$-2 sample, a SC of 430 F g^{-1} is obtained at 1 A g^{-1}, much less those than those of $NiCo_2O_4$-1 and the mesoporous hollow $NiCo_2O_4$ electrodes, which should be ascribed to its even thicker shell and mutually adhesive features. Unexpectedly, the SC retention of ~73% still can be maintained when the current density increased from 1 to 10 A g^{-1}, which should be related to the partial preservation of the appealing hollow nature.

In addition, further calculation of the pure EDLC by using the BET SSA of an average value of 20 μF cm^{-2} in ref. 32 and 33 delivers an EDLC of ~23 F g^{-1} for such unique hollow $NiCo_2O_4$ sub-microspheres, which is much lower than the corresponding measured SCs of 678 F g^{-1}. Therefore, it is further suggested that the main component of the measured SC is produced from the pseudocapacitive surface redox process and the Faradaic pseudocapacitances can be calculated as ~655 F g^{-1} (*i.e.*, 565 μF cm^{-2}) at 1 A g^{-1}, and even 565 μF cm^{-2} at 10 A g^{-1}, revealing its high surface utilization for rapid electrochemical energy storage at large current densities. The mesoporous hollow feature of the $NiCo_2O_4$ sub-microspheres renders rich and hierarchical diffusion channels, which reduce the diffusion length of electrolyte ions and ensure enough electrolyte ions to rapidly contact the ultrathin $NiCo_2O_4$ NS building blocks with rich electroactive sites. In particular, the hollow cavities, owing to its great role of ''ion-buffering reservoirs'',[13,20–22,34,35] can efficiently offer a robust conservation of OH^- ions and make sure that sufficient Faradaic reactions can take place at high current densities for energy storage. This in turn guarantees the better electrochemical utilization and the higher-rate charge–discharge performance.

Retention of the SC during long charge–discharge cycles at high current density operating conditions is essential for practical viability of ECs. Fig. 8 demonstrates the continuous charge–discharge assessment of unique hollow $NiCo_2O_4$ sub-microspheres electrode for 3500 cycles under a large current density of 10 A g^{-1}. Evidently, the discharge capacity gradually increases up to 559 F g^{-1} after ~300 cycles, instead of decreasing as in most cycle stability tests, that is to say, the additional 300 cycles are needed to fully activate the present sample. The decay in SC based on this maximum value after the following 3200-cycle test is ~13%, and then the SC remains at a stable value of 485 F g^{-1} with further cycling. Furthermore, the coulombic efficiency remains at ~100%

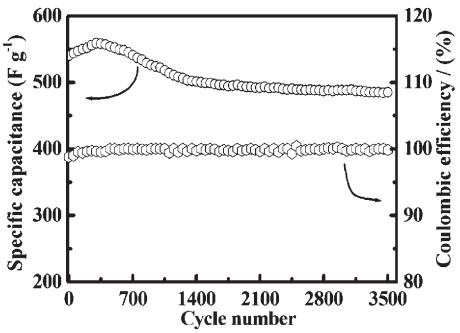

Fig. 8 Cycling performance and coulombic efficiency of the mesoporous hollow $NiCo_2O_4$ sub-microsphere electrode as a function of cycle number at 10 A g^{-1}.

during the consecutive cycles. Considering the large cost advantage of the present $NiCo_2O_4$ sample in contrast with the RuO_2, and its appealing electrochemical capacitance at high rates, mesoporous hollow $NiCo_2O_4$ sub-microspheres would be an excellent alternative material for next-generation ECs.

4. Conclusions

In summary, we developed an efficient template-engaged synthetic strategy to fabricate hierarchical $NiCo_2O_4$ mesoporous hollow sub-microspheres, which were assembled from ultrathin nanosheets with a thickness of a few nanometers. When utilized as an appealing electroactive material for ECs, the as-fabricated hierarchical $NiCo_2O_4$ hollow sub-microsphere electrode delivered a SC of 678 F g^{-1} at a current density of 1 A g^{-1}, and maintained it as high as 540 F g^{-1} even at 10 A g^{-1}. Furthermore, a desirable cycling stability of 13% SC degradation over 3500 continuous cycles at 10 A g^{-1} was observed, suggesting their promising application in advanced ECs. Our work opens up the possibility of constructing advanced but low-cost electrodes with high SC, excellent rate capability and remarkable cycling stability for next-generation ECs. More significantly, the electrode design concept can be easily generalized to other binary or even ternary metal oxides with unique hollow nano-/microstructures for high-performance ECs, or even advanced Li-ion batteries.

Acknowledgements

The authors acknowledge financial support from the National Natural Science Foundation of China (no. 51202004) and the Nature Science Foundation of Anhui Province (no. KJ2013A051).

References

1 T. Y. Wei, C. H. Chen, H. C. Chien, S. Y. Lu and C. C. Hu, *Adv. Mater.*, 2010, **22**, 347.
2 H. L. Wang, Q. M. Gao and L. Jiang, *Small*, 2011, **7**, 2454.
3 C. Z. Yuan, J. Y. Li, L. R. Hou, L. Yang, L. F. Shen and X. G. Zhang, *J. Mater. Chem.*, 2012, **22**, 16084.
4 H. Jiang, J. Ma and C. Z. Li, *Chem. Commun.*, 2012, **48**, 4465.
5 G. Q. Zhang and X. W. Lou, *Sci. Rep.*, 2013, **3**, 1470.
6 L. Yu, G. Q. Zhang, C. Z. Yuan and X. W. Lou, *Chem. Commun.*, 2013, **49**, 137.
7 G. Q. Zhang, H. B. Wu, H. E. Hoster, M. B. Chan-park and X. W. Lou, *Energy Environ. Sci.*, 2012, **5**, 9453.
8 G. Q. Zhang and X. W. Lou, *Adv. Mater.*, 2013, **25**, 976.
9 C. Z. Yuan, J. Y. Li, L. R. Hou, X. G. Zhang, L. F. Shen and X. W. Lou, *Adv. Funct. Mater.*, 2012, **22**, 4592.
10 C. H. Wang, X. Zhang, D. C. Zhang, C. Yao and Y. W. Ma, *Electrochim. Acta*, 2012, **63**, 220.
11 Y. Q. Wu, X. Y. Chen, P. T. Ji and Q. Q. Zhou, *Electrochim. Acta*, 2011, **56**, 7517.
12 Q. Lu, Y. P. Chen, W. F. Li, J. G. G. Chen, J. Q. Xiao and F. Jiao, *J. Mater. Chem. A*, 2013, **1**, 2331.
13 C. Z. Yuan, J. Y. Li, L. R. Hou, J. D. Lin, X. G. Zhang and S. L. Xiong, *J. Mater. Chem. A*, 2013, DOI: 10.1039/c3ta11949a.
14 J. W. Xiao and S. H. Yang, *RSC Adv.*, 2011, **1**, 588.
15 Q. F. Wang, B. Liu, X. F. Wang, S. H. Ran, L. M. Wang, D. Chen and G. Z. Shen, *J. Mater. Chem.*, 2012, **22**, 21647.
16 T. Wu, J. Y. Li, L. R. Hou, C. Z. Yuan, L. Yang and X. G. Zhang, *Electrochim. Acta*, 2012, **81**, 172.
17 L. F. Hu, L. M. Wu, M. Y. Liao, X. H. Hu and X. S. Fang, *Adv. Funct. Mater.*, 2012, **22**, 998.
18 M. R. Tarasevich and B. N. Efremov, in *Electrodes of Conductive Metallic Oxides Part A*, ed. S. Trasatti, Elsevier, USA, 1982, p. 227.
19 X. W. Lou, L. A. Archer and Z. C. Yang, *Adv. Mater.*, 2008, **20**, 3987.
20 X. Y. Lai, J. E. Halpert and D. Wang, *Energy Environ. Sci.*, 2012, **5**, 5604.
21 C. Z. Yuan, B. Gao, L. F. Shen, S. D. Yang, L. Hao, X. J. Lu, F. Zhang, L. J. Zhang and X. G. Zhang, *Nanoscale*, 2011, **3**, 529.
22 C. Z. Yuan, X. G. Zhang, L. H. Su, B. Gao and L. F. Shen, *J. Mater. Chem.*, 2009, **19**, 5772.
23 T. Zhu, Z. Y. Wang, S. J. Ding, J. S. Chen and X. W. Lou, *RSC Adv.*, 2011, **1**, 397.
24 W. Stöber, A. Fink and E. Bohn, *J. Colloid Interface Sci.*, 1968, **26**, 62.
25 N. Venkatathri and J. W. Yoo, *Bull. Korean Chem. Soc.*, 2008, **29**, 29.
26 C. C. Hu, K. H. Chang and C. C. Wang, *Electrochim. Acta*, 2007, **52**, 4411.
27 X. Wang, X. D. Han, M. F. Lim, N. Singh, C. L. Gan, J. Ma and P. S. Lee, *J. Phys. Chem. C*, 2012, **116**, 12448.
28 V. Gupta, S. Gupta and N. Miura, *J. Power Sources*, 2008, **175**, 680.
29 C. C. Hu and C. Y. Cheng, *Electrochem. Solid-State Lett.*, 2002, **5**, A43.
30 G. X. Hu, C. H. Tang, C. X. Li, H. M. Li, Y. Wang and H. Gong, *J. Electrochem. Soc.*, 2011, **158**, A695.
31 C. Z. Yuan, H. B. Wu, Y. Xie and X. W. Lou, *Angew. Chem., Int. Ed.*, 2013, DOI: 10.1002/anie.201303971.
32 L. Cao, M. Lu and H. L. Li, *J. Electrochem. Soc.*, 2005, **152**, A871.
33 H. Q. Li, J. Y. Luo, X. F. Zhou, C. Z. Yu and Y. Y. Xia, *J. Electrochem. Soc.*, 2007, **154**, A731.
34 D. W. Wang, F. Li, M. Liu, G. Q. Lu and H. M. Cheng, *Angew. Chem., Int. Ed.*, 2008, **47**, 373–376.
35 Q. Lu, J. G. Chen and J. Q. Xiao, *Angew. Chem., Int. Ed.*, 2013, **52**, 1882.

